Fırat Üniversitesi Deneysel ve Hesaplamalı Mühendislik Dergisi

FUJECE

Hareketli Kayma Yüzeyli DC Motor Modelli Klasik Kayan Kipli Kontrolün Dönel Ters Sarkaç Sistemine Uygulanması

Muhammet AYDIN[1*], Oğuz YAKUT[2]

[1, 2]Mechatronics Engineering, Faculty of Engineering, Firat University, Elazığ, Türkiye.
[1]muhammeta@firat.edu.tr, [2]oyakut@firat.edu.tr

Geliş Tarihi: 01.03.2024
Kabul Tarihi: 11.07. 2024

Düzeltme Tarihi: 22.05.2024

doi: 10.62520/fujece.1445734
Araştırma Makalesi

Alıntı: M. Aydın ve O. Yakut, "Hareketli kayma yüzeyli dc motor modelli klasik kayan kipli kontrolün dönel ters sarkaç sistemine uygulanması", Fırat Üni. Deny. ve Hes. Müh. Derg., vol. 3, no 3, pp. 337-349, Ekim 2024.

Öz

Bu çalışmada kontrol uygulamalarında çok tercih edilen dönel ters sarkaç sistemi (DTS) ele alınmıştır. DTS elemanlarının ağırlık merkezi koordinatları bulunarak sistemin toplam kinetik ve potansiyel enerjileri elde edilmiştir. Kinetik ve potansiyel enerji ifadeleri kullanılarak Lagrange fonksiyonu oluşturulmuştur. Lagrange yöntemi dikkate alınarak sistemin hareket denklemlerini veren ifadeler bulunmuştur. Ayrıca sistemi harekete geçirecek olan motorun denklemleri dikkate alınmıştır. Durum değişkenleri kullanılarak Matlab da yazılan program yardımıyla sistemin sarkaç açısı, kayma yüzeyi hareketli klasik kayan kipli kontrol yöntemiyle kontrol edilmiştir. Kayma yüzeyinin eğimi sistemin dinamiklerine bağlı olarak hesaplatılmıştır. Kontrol yapısında kullanılan katsayıların optimum değerleri genetik algoritma yardımıyla bulunmuştur. Sonuçlardan sarkaç açısının istenilen referans değere yaklaşık 1.5 sn civarında ulaştığı ve hatanın yaklaşık sıfır olduğu görülmüştür. Ayrıca motor tork değerinin 12 Nm seviyelerinde ve motor akım değerinin 2.5 amper seviyelerinde olduğu gözlemlenmiştir. Motor değerlerinin pratik uygulamalardaki değerlere yakın makul seviyelerde olduğu sonuçlardan elde edilmiştir. Elde edilen bu değerlere göre motor seçimi yapıldığında gerçek zamanlı uygulamalarda kontrol için sorun yaşanmayacaktır.

Anahtar kelimeler: Dönel ters sarkaç, Hareketli kayan kipli kontrol, Kayma yüzeyi, Motor model

*Yazışılan yazar

İntihal Kontrol: Evet – Turnitin
Şikayet: fujece@firat.edu.tr

Firat University Journal of Experimental and Computational Engineering

FUJECE

An Application of DC Motor Modelled Classical Sliding Mode Control with Moving Sliding Surface to Rotary Inverted Pendulum System

Muhammet AYDIN[1*], Oğuz YAKUT[2]

[1, 2]Mechatronics Engineering, Faculty of Engineering, Firat University, Elazığ, Türkiye.
[1]muhammeta@firat.edu.tr, [2]oyakut@firat.edu.tr

Received: 01.03.2024
Accepted: 11.07. 2024
Revision: 22.05.2024
doi: 10.62520/fujece.1445734
Research Article

Citation: M. Aydın ve O. Yakut, "A comparative study of segmentation algorithms for ıntracerebral hemorrhage detection", Firat Univ. Jour.of Exper. and Comp. Eng., vol. 3, no 2, pp. 337-349, October 2024.

Abstract

The rotary inverted pendulum system (RIP), which is highly favored in control applications, is examined in this work. By determining the coordinates of the Rip elements' centers of gravity, the system's total kinetic and potential energies were determined. The kinetic and potential energy expressions were used to generate the Lagrangian function. Expressions providing the system's equations of motion were discovered by taking the Lagrangian approach into consideration. The motor's equations, which will initiate the system, have also been considered. Through the use of state variables and a Matlab program, the system's pendulum angle was managed by using a moving sliding surface and the traditional sliding mode control technique. Based on the dynamics, the slip surface's slope was computed. The sliding surface's slope was computed based on the system's dynamics. The genetic algorithm was utilized to determine the ideal values for the coefficients employed in the control structure. The findings showed that the inaccuracy was roughly zero and that the pendulum angle took around 1.5 seconds to reach the intended reference value. Furthermore, it noted that the motor torque and current values are 12 Nm and 2.5 amps, respectively. The findings show that the motor values are reasonably similar to the values seen in real-world applications. Control in real-time applications won't be an issue if the motor is chosen based on these values.

Keywords: Rotary inverted pendulum, Moving sliding mode control, Sliding surface, Motor model

*Corresponding author

1. Introduction

One of the most popular approaches for applying control techniques is the inverted pendulum system because of their challenging controllability. Among the inverted pendulum systems created to date are single rod trolley and rotary inverted pendulum systems, double rod trolley and rotary inverted pendulum systems [1-4].

The rotary inverted pendulum (rip) system is among the inverted pendulum systems that are used most frequently. A valuable test system for investigating the control of nonlinear unstable systems is the inverted pendulum system driven indirectly, often referred to as the "rip system." In recent years, the rip has become standard for applications in control due to its lower cost and easier construction than the trolley inverted pendulum system. The pendulum of the rip system rotates vertically, while the rotary arm moves horizontally. The rotating arm is propelled by the DC motor. It is tried to stabilize the rotary arm-mounted pendulum at the higher equilibrium point, or the point of instability, subsequent to the rotary arm's movement by the DC motor [5, 6].

There are studies published in the literature so far on the angle control of the rotary inverted pendulum system shown in Figure 1. The prominent ones among these are the studies using classical control methods such as PID, PI, PD, sliding mode controlled adaptive control methods, fuzzy control method, sliding mode control method, particle swarm optimization based PID control and artificial neural network sliding mode control methods [7-22].

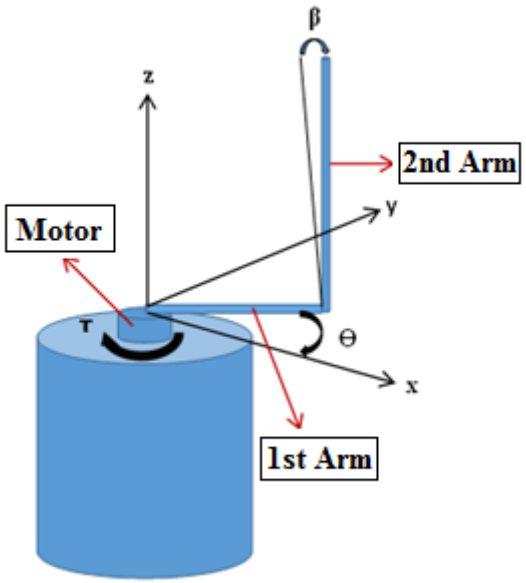

Figure 1. Rotational inverted pendulum system

In this paper, a nonlinear mathematical system of the rip is obtained and the sliding mode control method with moving sliding surface is used to control the pendulum. The dynamics of the system are employed to derive the slope of the sliding surface. The optimization method using genetic algorithms is then applied to calculate the required coefficients for the control system.

2. Modelling of Rotational Inverted Pendulum System

A single motor powers the two-degree-of-freedom system shown in Figure 1. The system's changeable parameters are Θ and β. Figure 1 displays the system's coordinate axis layout. If this coordinate axis set is used to determine the system's total kinetic energy;

$$T = \frac{1}{2}m_1\left(\dot{x}_1{}^2 + \dot{y}_1{}^2\right) + \frac{1}{2}I_1\dot{\theta}^2 + \frac{1}{2}m_2\left(\dot{x}_2{}^2 + \dot{y}_2{}^2 + \dot{z}_2{}^2\right) + \frac{1}{2}I_2\dot{\beta}^2 \quad (1)$$

In the equations x_1, y_1 are the centre of gravity coordinates of the first arm. x_2 , y_2 and z_2 represent the the second arm's coordinates for center of gravity. m_1 and m_2 are the masses of each arm. I_1 and I_2 are the mass moments of inertia of the arms. L_1 and L_2, respectively, are the limb dimensions of arms. The coefficients of friction at the joint joints are b_1 and b_2. τ is the control torque applied by the motor.
Equations (1) yields the following equations for the unknown expressions.

$$x_1 = L_1 cos\theta \quad (2)$$

$$y_1 = L_1 sin\theta \quad (3)$$

$$x_2 = x_1 - L_2 \sin\beta\sin\theta \quad (4)$$

$$y_2 = y_1 + L_2 sin\beta cos\theta \quad (5)$$

$$z_2 = L_2 cos\beta \quad (6)$$

If the aforementioned equations are changed to determine the system's total kinetic energy;

$$T = \frac{1}{2}m_1{L_1}^2\dot{\theta}^2 + \frac{1}{2}I_1\dot{\theta}^2 + \frac{1}{2}m_2\left(L_1\dot{\theta}^2 + 2L_1L_2cos\beta\dot{\theta}\dot{\beta} + {L_2}^2\dot{\beta}^2 + {L_2}^2sin^2\beta\dot{\theta}^2\right) + \frac{1}{2}I_2\dot{\beta}^2 \quad (7)$$

Potential energy of the system:

$$V = m_2 g z_2 \quad (8)$$

$$V = m_2 g L_2 cos\beta \quad (9)$$

This gives rise to the following construction of the Lagrange function.

$$L = T - V \quad (10)$$

$$L = \frac{1}{2}\left(m_1{L_1}^2 + I_1\right)\dot{\theta}^2 + \frac{1}{2}m_2\left[\left(L_1 + {L_2}^2sin^2\beta\right)\dot{\theta}^2 + 2L_1L_2cos\beta\dot{\theta}\dot{\beta} + {L_2}^2\dot{\beta}^2\right] + \frac{1}{2}I_2\dot{\beta}^2 - m_2gL_2cos\beta \quad (11)$$

Equation of motion for θ:

$$\frac{d}{dt}\left(\frac{\partial L}{\partial\dot{\theta}}\right) - \frac{\partial L}{\partial\theta} = Q_\theta \quad (12)$$

The equation of motion for θ can be found by substituting and calculating the expressions in the equation.

$$\left(m_1{L_1}^2 + I_1 + m_2L_1 + m_2{L_2}^2sin^2\beta\right)\ddot{\theta} + m_2L_1L_2cos\beta\ddot{\beta} - m_2L_1L_2sin\beta\dot{\beta}^2 + 2m_2{L_2}^2sin\beta cos\beta\dot{\beta}\dot{\theta} = \tau - b_1\dot{\theta} \quad (13)$$

Equation of motion for β:

$$\frac{d}{dt}\left(\frac{\partial L}{\partial\dot{\beta}}\right) - \frac{\partial L}{\partial\beta} = Q_\beta \quad (14)$$

Here is the equation of motion for β after performing the appropriate operations in the preceding equation.

$$m_2L_1L_2cos\beta\ddot{\theta} + \left(m_2{L_2}^2 + I_2\right)\ddot{\beta} - m_2{L_2}^2sin\beta cos\beta\dot{\theta}^2 - m_2gL_2sin\beta = -b_2\dot{\beta} \quad (15)$$

After extracting $\ddot{\beta}$ and $\ddot{\theta}$ expressions from the equations of motion, the following equations are produced.

$$\ddot{\theta} = \frac{\left(m_2{L_2}^2 + I_2\right)\left(b_1\dot{\theta} - \tau - m_2L_1L_2sin\beta\dot{\beta}^2 + 2m_2{L_2}^2sin\beta cos\beta\dot{\beta}\dot{\theta}\right)}{(m_2L_1L_2cos\beta)^2 - \left(m_2{L_2}^2 + I_2\right)\left(m_1{L_1}^2 + I_1 + m_2L_1 + m_2{L_2}^2sin^2\beta\right)}$$

$$- \frac{m_2L_1L_2cos\beta\left(b_2\dot{\beta} - m_2{L_2}^2sin\beta cos\beta\dot{\theta}^2 - m_2gL_2sin\beta\right)}{(m_2L_1L_2cos\beta)^2 - \left(m_2{L_2}^2 + I_2\right)\left(m_1{L_1}^2 + I_1 + m_2L_1 + m_2{L_2}^2sin^2\beta\right)} \quad (16)$$

$$\ddot{\beta} = \frac{\left(m_1{L_1}^2 + I_1 + m_2L_1 + m_2{L_2}^2sin^2\beta\right)\left(b_2\dot{\beta} - m_2{L_2}^2sin\beta cos\beta\dot{\theta}^2 - m_2gL_2sin\beta\right)}{(m_2L_1L_2cos\beta)^2 - \left(m_2{L_2}^2 + I_2\right)\left(m_1{L_1}^2 + I_1 + m_2L_1 + m_2{L_2}^2sin^2\beta\right)}$$

$$- \frac{m_2L_1L_2cos\beta\left(b_1\dot{\theta} - \tau - m_2L_1L_2sin\beta\dot{\beta}^2 + 2m_2{L_2}^2sin\beta cos\beta\dot{\beta}\dot{\theta}\right)}{(m_2L_1L_2cos\beta)^2 - \left(m_2{L_2}^2 + I_2\right)\left(m_1{L_1}^2 + I_1 + m_2L_1 + m_2{L_2}^2sin^2\beta\right)} \quad (17)$$

The DC motor responsible for the first arm's rotational movement has the following equation of motion. Where L is the motor inductance coefficient, N is the gear ratio, I is the electrical current flowing through the motor windings, R is the motor winding ohmic resistance, and V_a is the motor supply voltage and control signal. The opposite electromotive voltage coefficient is denoted by K_b.

$$\frac{di}{dt} = \frac{V_a - Ri}{L} - \frac{K_b\dot{\theta}}{LN} \quad (18)$$

Should we change the equations' expressions into state variables;

$$\theta = x(1) \quad (19)$$

$$\dot{\theta} = x(2) \quad (20)$$

$$\beta = x(3) \quad (21)$$

$$\dot{\beta} = x(4) \quad (22)$$

$$i = x(5) \quad (23)$$

is acquired as. If the torque used for motor control is;

$$\tau = \frac{K_t i}{N} \quad (24)$$

is computed using the format. The motor torque coefficient in this case is K_t.

A Matlab programme is used to apply a approach to movable sliding mode control for the rip system by using these variables of state. It is guaranteed that β will reach the intended zero reference point when using moving sliding mode control approach. Table 1 provides the numerical values for the system parameters.

Table 1. Values for rip system parameters

Parameter	Value	Unit
m_1	0.15	kg
m_2	0.1	kg
L_1	0.4	m
L_2	0.4	m
b_1	0.01	Ns/m
b_2	0.01	Ns/m
I_1	0.0248	kgm^2
I_2	0.00386	kgm^2
L	0.1	Henry
R	1.4	Ohm
K_t	0.25	---
K_b	0.05	---
N	1/20	---

3. Classical Sliding Mode Control Design with Moving Sliding Surface

A reliable and nonlinear control technique is sliding mode control. Unlike other control systems, it is unaffected by outside disruptions. It can rapidly and accurately approach the desired reference because of the vibrations on the sliding surface [23]. When the system's boundary values are known, sliding mode control offers long-term controllability in situations when the system's parameters are dynamic or uncertain as well as when external disturbances affect the system.

Before implementing sliding mode control, it is imperative to determine the location of the sliding surface and establish a control rule that ensures reaching this identified surface. The reaching time denotes the duration required to reach the sliding surface, and the phase trajectory section during this process is referred to as the reaching mode. During the reaching mode, the plant is susceptible to external noise and uncertainties in parameters [24]. Upon achieving the sliding surface, the system transitions into the sliding mode. In this mode, the system's trajectory remains unaffected by external variables and unpredictable parameters. The application of sliding mode control unveils previously unrepresented high-frequency dynamics of the system, manifesting as crackling. This phenomenon arises from oscillations near the equilibrium point that the system is endeavoring to reach.
Control expression in sliding mode using sign function;

$$U = -k\ sign(S) \tag{25}$$

is able to communicate as slip surface function (S) in this case is represented by equation (26) and is dependent on the error (e) and its time variation (de) with respect to the system's response.

$$S = C\ e + de \tag{26}$$

Figure 2 shows a sliding surface example for the sliding mode control. The sliding surface's precise slope is depicted in the illustration. In equation (26), the coefficient C provides this slope.

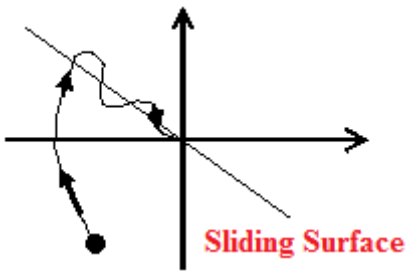

Figure 2. Sliding surface

The ideal slope value must be found in order to guarantee the controller's success. These sliding surface slope coefficients of the sliding mode controller are assumed to be shifting in this study. Expression (27) is used to get the slope coefficient C instantly. Here, the evolutionary algorithm was used to determine the constant coefficients C1 and C2's optimal values. As a result, the slope of sliding surface coefficient for the sliding mode control was instantly determined.

$$C = C_1 - C_2 \frac{de}{e} \tag{27}$$

The main applications of genetic algorithms are in machine learning and problem optimization, among many other areas. The process of making something better than it was before is called optimization. In optimization, a set of inputs is given, and the outcome is determined by the inputs. In order for optimization to produce the "best" result, we must provide an insert. The precision of "best" depends on the different types of the problem [25]. The parameters preferred as FitnessLimit 1e-10, Generations 100, and PopulationSize 20 in the genetic algorithm structure. The block design for the genetic algorithm technique used to optimize the controller's coefficients is displayed in Figure 3.

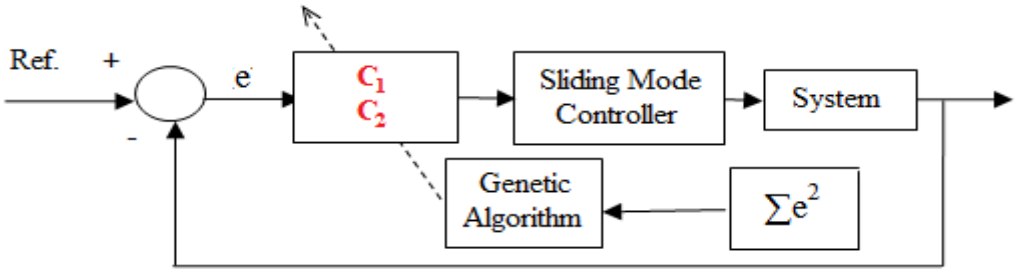

Figure 3. Controller block diagram

There is a shifting sliding surface in our control approach since the obtained coefficient C will change every time. Figure 4 displays the C coefficient's mobility.

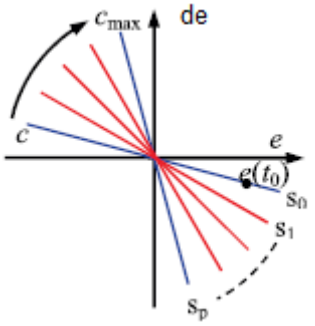

Figure 4. C coefficient variation

For the fitness function, the mean squared error criterion—which is also known as the system performance index—is favored in order to determine the ideal controller parameter values.

$$E(k) = \frac{1}{2}e^2(k) \tag{28}$$

The sliding mode control expression's signalling function results in a crackling control signal. Various functions are employed in place of the sign function in order to solve this issue. In this study, the sign function is replaced with the commonly utilized saturation function. As a result, it is computed to obtain the expression for the regulation of the sliding mode with saturation function. Here, genetic algorithm determines epsilon value to be 37.77.

$$U = -k.sat(\frac{S}{Epsilon}) \tag{29}$$

4. Results and Discussion

The results obtained as a result of the study were examined respectively. Figure 5 illustrates the temporal evolution of the angular position of the first arm, connected to the motor, over time. The motion commences from the zero-point and undergoes a change in direction within the initial seconds. This observed change corresponds with the anticipated outcome when elevating the pendulum.

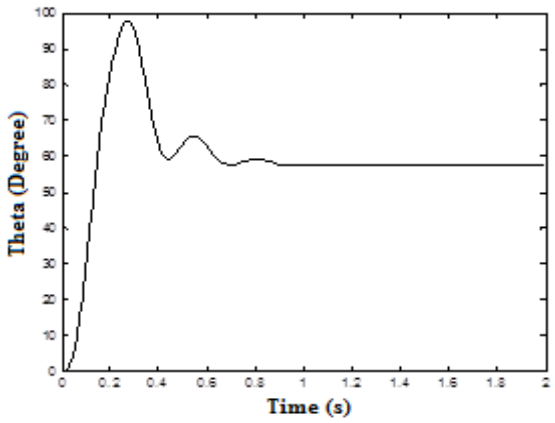

Figure 5. Theta angle variation in relation to time

The graphical representation of the angular velocity of the first arm is depicted in Figure 6 over time. The graph showcases oscillations in angular velocity, reaching a maximum of 11 rad/s before eventually stabilizing at 0 rad/s.

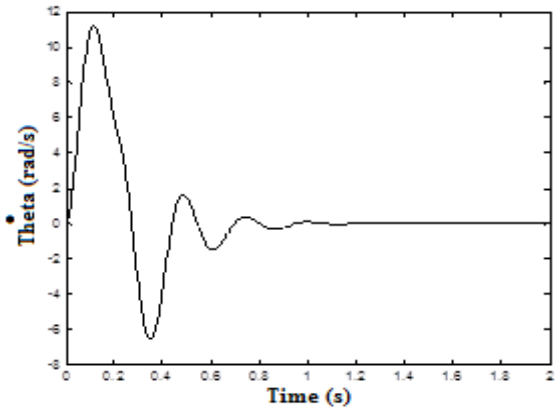

Figure 6. Change in the first arm's angular velocity to time

In Figure 7, the graph illustrates the variation in the pendulum angle over time. The unstable upper equilibrium point is where the pendulum is expected to cease movement. Therefore, the pendulum angle should approach the intended zero reference point. According to the visual data, it takes approximately 1.5 seconds for the pendulum to reach the target reference value.

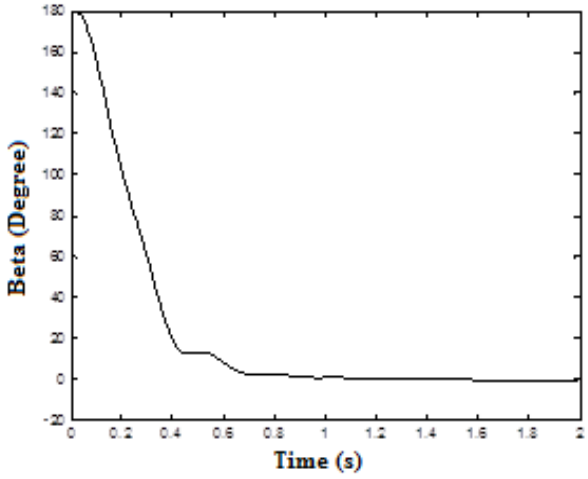

Figure 7. Beta angle (pendulum angle) variation to time

The pendulum's angular velocity fluctuates with regard to time, as seen in Figure 8. The graph indicates that, in 1.5 seconds, the pendulum's angular velocity goes to zero.

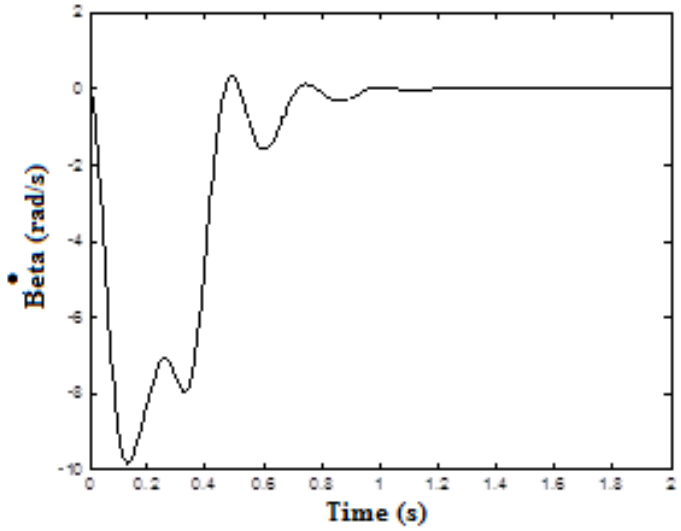

Figure 8. Beta angle (pendulum angle) variation to time

Figure 9 portrays the torque values that the DC motor should apply to the first arm and the slope values of the sliding surface, respectively. It is clear from examining the DC motor torque curve in Figure 9 shows that the pendulum may be raised to the required reference value with a motor torque of roughly 12 Nm. In light of realistic applications, it can be said that this torque value makes sense. Approximately 1.5 seconds pass before the motor torque drops to zero.

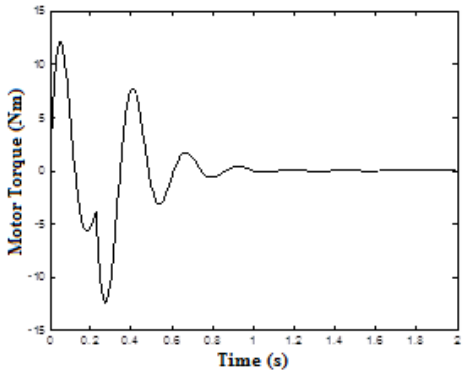

Figure 9. Changes in DC motor torque over time

Figure 10 shows the data from the slope graph of the sliding surface.

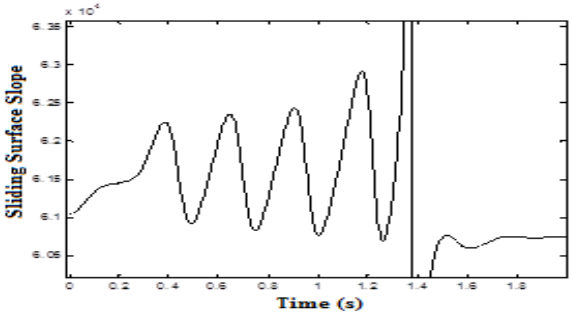

Figure 10. Sliding surface slope graph

The supply voltage variation over time that will be used as a control signal for the DC motor is depicted in Figure 11. The graph indicates that the maximum voltage source for the DC motor supply is 12 volts.

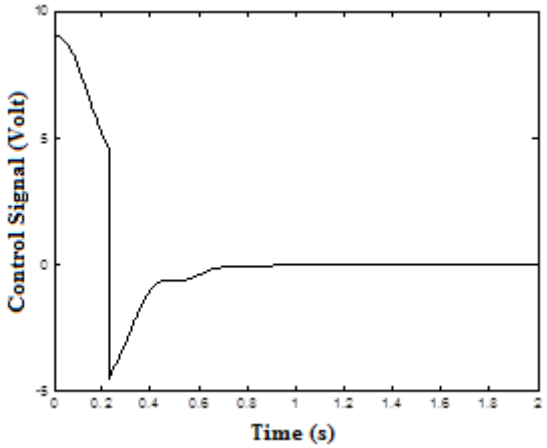

Figure 11. DC motor control signal change graph over time

Figure 12 illustrates the temporal variation of the current flowing through the DC motor windings. It is apparent that, after approximately 1.5 seconds, the motor ceases to draw any current. The graph clearly indicates that the motor is limited to drawing a maximum of 2.5 amps of electricity.

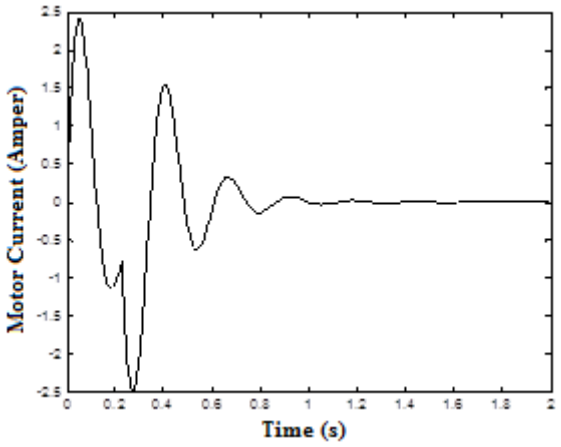

Figure 12. Graph of DC motor current change with time

In Table 2, the results of the study conducted in this research article and a publication in the literature are compared [26]. As can be seen in the table, the pendulum angle of the system achieved a better settling time of 0.9 s in the current study.

Table 2. Comparison of between the literature and the present work

	Method	**Settling Time (s)**
Rotary inverted pendulum arm angle	SMC	0.89
	MSMC (Present Work)	**0.85**
Pendulum angle	SMC	1.2
	MSMC (Present Work)	**0.90**

5. Conclusion

The initial phase of this study involves the application of the Lagrange technique to formulate the nonlinear model for a single-degree-of-freedom spinning inverted pendulum system. The control of the pendulum angle is conducted through Matlab software, utilizing state variables within the final model. This control is achieved by implementing the moving sliding mode technique. The dynamics of the system were computed, revealing variations in the slope of the sliding surface. To determine the coefficients in the structure of the sliding modal control, a genetic algorithm was employed. As a result, the identified error was rectified, leading to a control signal reduction to zero. According to the investigation, the pendulum took approximately 1.5 seconds to reach the specified reference value. Notably, the motor's characteristics, including a maximum torque of 12 Nm and a maximum power consumption of 2.5 amps, were documented. These findings underscore the successful application of moving sliding mode control to the system, provided that motor selection is performed by considering real-time motor values during the selection process.
In future studies, moving sliding mode control method is considered to be applied to many robotic systems. Since the moving sliding mode control method gives better results than the classical sliding mode control, it will be a robust and better control method in other systems where it will be applied.

6. Author Contribution Declaration

Author 1 developed the concept for the study, derived the system's dynamic equations, obtained the state space equations, evaluated the results, reviewed the literature, checked for spelling errors, and ensured the article's content was correct. Author 2 developed the system's software program, obtained the program's result graphics, evaluated the results, checked for spelling errors, and ensured the article's content was correct.

7. Ethics Committee Approval and Conflict of Interest Declaration

Ethics committee permission is not required for the prepared article. There is no conflict of interest with any person/institution in the prepared article.

8. References

[1] M. Bugeja, "Non-linear swing-up and stabilizing control of an inverted pendulum system," The IEEE Region 8 EUROCON 2003. Computer as a Tool., Ljubljana, Slovenia, pp. 437-441, vol. 2, 2003.
[2] W. Zhong and H. Rock, "Energy and passivity based control of the double inverted pendulum on a cart," in Proceedings of the 2001 IEEE International Conference on Control Applications (CCA'01), Mexico City, Mexico, pp. 896-901, 2001.
[3] J. Krishen and V. M. Becerra, "Efficient fuzzy control of a rotary inverted pendulum based on LQR mapping," in Proceedings of the 2006 IEEE Conference on Computer Aided Control System Design, 2006 IEEE International Conference on Control Applications, 2006 IEEE International Symposium on Intelligent Control, Munich, Germany, pp. 2701-2706, 2006.
[4] S. Awtar, N. King, T. Allen, I. Bang, M. Hagan, D. Skidmore, K. Craig, "Inverted pendulum systems: rotary and arm-driven - a mechatronic system design case study," Mechat., vol. 12, no. 2, pp. 357-370, 2002.
[5] Q. Yan, "Output tracking of underactuated rotary inverted pendulum by nonlinear controller," in Proceedings of the 42nd IEEE International Conference on Decision and Control (IEEE Cat. No.03CH37475), Maui, HI, USA, vol. 3, pp. 2395-2400, 2003.
[6] T. C. Kuo, Y. J. Huang, and B. W. Hong, "Adaptive PID with sliding mode control for the rotary inverted pendulum system," in Proceedings of the 2009 IEEE/ASME International Conference on Advanced Intelligent Mechatronics, Singapore, pp. 1804-1809, 2009.
[7] J. Nuo and H. Wang, "Nonlinear Control of an Inverted Pendulum System based on Sliding mode method," ACTA Analy. Funct. Appl., vol. 9, no. 3, pp. 234-237, 2008.
[8] J. Krishen and V. M. Becerra, "Efficient fuzzy control of a rotary inverted pendulum based on LQR mapping," in Proceedings of the 2006 IEEE Conference on Computer Aided Control System Design, 2006 IEEE International Conference on Control Applications, 2006 IEEE International Symposium on Intelligent Control, Munich, Germany, pp. 2701-2706, 2006.
[9] O. Altinoz, A. Tolga, E. Yilmaz, and G. W. Weber, "Chaos particle swarm optimized PID controller for the inverted pendulum system," in Proceedings of the 2nd international conference on engineering optimization, 2010.
[10] S. Toshiharu and K. Fujimoto, "Controller design for an inverted pendulum based on approximate linearization," International Journal of Robust and Nonlinear Control: IFAC-Affiliated Journal, vol. 8, no. 7, pp. 585-597, 1998.
[11] M. A. Khanesar, M. Teshnehlab, and M. A. Shoorehdeli, "Fuzzy Sliding Mode Control of Rotary Inverted Pendulum," in Proceedings of the 2007 IEEE International Conference on Computational Cybernetics, Gammarth, Tunisia, pp. 57-62, 2007.
[12] W. Wang, "Adaptive fuzzy sliding mode control for inverted pendulum," in Proceedings of the 2009 International Symposium on Computer Science and Computational Technology (ISCSCI 2009), Academy Publisher, pp. 231, 2009.
[13] A. Bogdanov, "Optimal control of a double inverted pendulum on a cart," Oregon Health and Science University, Tech. Rep. CSE-04-006, OGI School of Science and Engineering, Beaverton, OR, 2004.
[14] I. Hassanzadeh and S. Mobayen, "PSO-based controller design for rotary inverted pendulum system," Jour. of Appl. Sci., vol. 8, no. 16, pp. 2907-2912, 2008.
[15] V. Sukontanakarn and M. Parnichkun, "Real-time optimal control for rotary inverted pendulum," American Journal of Applied Sciences, vol. 6, no. 6, pp. 1106, 2009.
[16] M. Aydın, O. Yakut, and H. Tutumlu, "Implementation of the network-based moving sliding mode control algorithm to the rotary inverted pendulum system," Jour. of Eng. and Techn., vol. 3, no. 1, pp. 31-40, 2009.

[17] S. Horikawa, T. Furuhashi, and Y. Uchikawa, "Fuzzy control for inverted pendulum using fuzzy neural networks," J. Rob. and Mechat., vol. 7, no. 1, pp. 36-44, 1995.
[18] I. H. Zadeh and S. Mobayen, "PSO-based controller for balancing rotary inverted pendulum," J. Appl. Sci., vol. 16, pp. 2907-2912, 2008.
[19] S. D. Sanjeewa and M. Parnichkun, "Control of rotary double inverted pendulum system using LQR sliding surface based sliding mode controller," Jour. of Con. and Dec., vol. 9, no. 1, pp. 89-101, 2022.
[20] A. Ma'arif, M. A. M. Vera, M. S. Mahmoud, S. Ladaci, A. Çakan, and J. N. Parada, "Backstepping sliding mode control for inverted pendulum system with disturbance and parameter uncertainty," Jour. of Robotics and Con. (JRC), vol. 3, no. 1, pp. 86-92, 2022.
[21] R. Hernández and F. Jurado, "Adaptive Neural Sliding Mode Control of an Inverted Pendulum Mounted on a Ball System," in Proceedings of the 2018 15th International Conference on Electrical Engineering, Computing Science and Automatic Control (CCE), Mexico City, Mexico, pp. 1-6, 2018.
[22] S. Irfan, A. Mehmood, M. T. Razzaq, and J. Iqbal, "Advanced sliding mode control techniques for inverted pendulum: Modelling and simulation," Eng. Sci. and Techn., an Inter. Jour., vol. 21, no. 4, pp. 753-759, 2018.
[23] K. D. Young, V. I. Utkin, and U. A. Ozguner, "Control engineer's guide to sliding mode control," IEEE Transactions on Control Systems Technology, vol. 7, no. 3, pp. 328-342, 1999.
[24] C. Edwards and S. K. Spurgeon, Sliding Mode Control: Theory and Applications, New York: Taylor and Francis, 1998.
[25] Chuan-Kang Ting, "On the Mean Convergence Time of Multi-parent Genetic Algorithms without Selection," in Advances in Artificial Life, Springer, Berlin, Heidelberg, pp. 403-412, 2005.
[26] K. Nath and L. Dewan, "A comparative analysis of linear quadratic regulator and sliding mode control for a rotary inverted pendulum," in Proceedings of the 2018 International Conference on Recent Trends in Electrical, Control and Communication, pp. 302-307, 2018.